Anisotropic and Passivation-Dependent Quantum Confinement Effects in Germanium Nanowires: A Comparison with Silicon Nanowires

Mingwei Jing,[†] Ming Ni,[†] Wei Song,[†] Jing Lu,*[,†,‡] Zhengxiang Gao,*[,†] Lin Lai,[†] Wai Ning Mei,[‡] Dapeng Yu,[†] Hengqiang Ye,[†] and Lu Wang[†]

Mesoscopic Physics Laboratory, Department of Physics, Peking University, Beijing 100871, PRC, and Department of Physics, University of Nebraska at Omaha, Omaha, Nebraska 68182-0266

Received: June 7, 2006; In Final Form: July 28, 2006

Electronic structures of hydrogen-passivated germanium nanowires (GeNWs) along the [100], [110], [111], and [112] directions are studied by using the density functional theory within the generalized gradient approximation. The band gaps of the fully relaxed GeNWs along the [100], [110], and [111] directions are all direct at the smaller sizes, while those of the wires along the [112] direction remain indirect. The magnitude of the band gaps of the GeNWs for a given size approximately follows the order of $E_g[100] > E_g[111] > E_g[112] > E_g[110]$. Compared with silicon nanowires, GeNWs exhibit stronger quantum confinement effects. Replacement of H by the more stable ethine group is found to lead to a weakening of the quantum confinement effects of GeNWs.

Introduction

Quasi-one-dimensional structures of semiconductor have attracted much attention due to significant technological implications[1,2] and theoretical significance. Silicon nanowires (SiNWs) have been explored and studied both experimentally[3−5] and theoretically[6−10] for a long time. Different from bulk Si with an indirect energy gap of 1.17 eV, SiNWs can possess direct energy gaps[6−10] and strong luminescent properties[11] in the visible light range, which has potential applications in optoelectronic devices. Germanium is a congener of Si, and germanium nanowires (GeNWs) could be used in optoelectronic components fabricated within silicon technology. Compared with Si, Ge has a smaller indirect band gap of 0.74 eV, a higher carrier mobility, a larger dielectric constant, and a larger excitonic Bohr radius (243 and 49 Å for Ge and Si, respectively[12,13]). The larger excitonic Bohr radius of Ge implies more prominent quantum confinement effects of Ge than Si, and this has been confirmed when they are confined in three dimensions by comparing the measured conduction band edge shift between similar-sized Ge and Si nanocrystals.[14] It is interesting to check whether the stronger quantum confinement effects for Ge than for Si also occur when they are confined in two dimensions.

Although a variety of techniques have been developed to synthesize GeNWs,[15−17] theoretical research on low-dimensional germanium structures is mainly focused on quantum dots[18−22] and quantum films.[23−25] The electronic structures and optical properties of the hydrogen-passivated GeNWs along the [100], [110], and [111] directions with effective widths d (defined as the cross-section linear parameter) of 4, 8, and 12 Å were studied recently[26,27] by using the density functional theory (DFT) within the local density approximation (LDA) plus the GW approximation correction to the LDA band gap. In the two works, the geometry of the GeNWs is either not relaxed[26] or only relaxed for the atomic positions but not for the wire axis.[27] These studies reveal that the band gaps of the GeNWs are enlarged with the decreasing wire size, which results in a shift of the overall optical absorption spectra toward higher frequency. The [110]-oriented

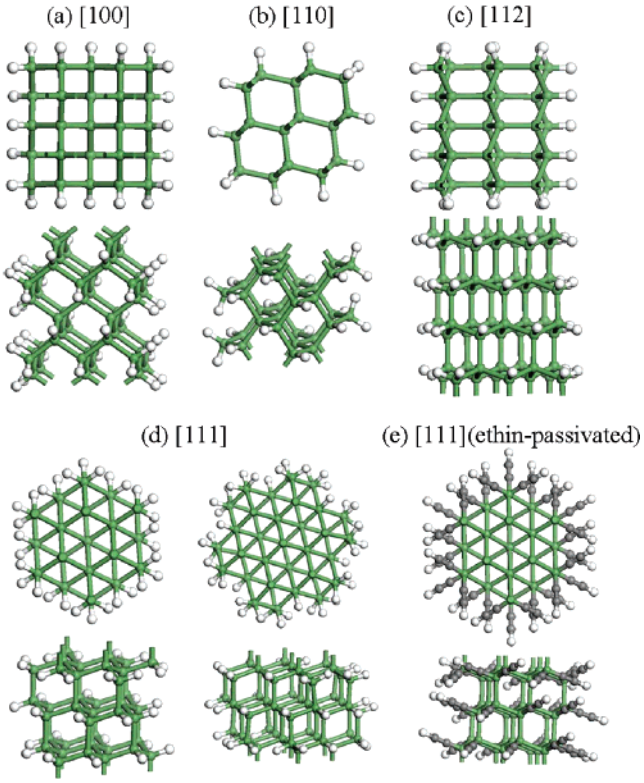

Figure 1. (Color online) Structures of the GeNWs viewed from top (upper) and side (lower): (a)−(d) the H-passivated GeNWs along the [100], [110], [112], and [111] directions, respectively, and (e) the ethine-passivated GeNW along the [111] direction. The wires along the [111] direction have hexagonal (left) and starlike (right) two types of cross sections. Green, white, and gray balls indicate Ge, H, and C atoms, respectively.

* Corresponding authors. E-mail: (Lu) jinglu@pku.edu.cn; (Gao) zxgao@pku.edu.cn.
[†] Peking University.
[‡] University of Nebraska at Omaha.

10.1021/jp063518j CCC: $33.50
Published on Web 08/29/2006

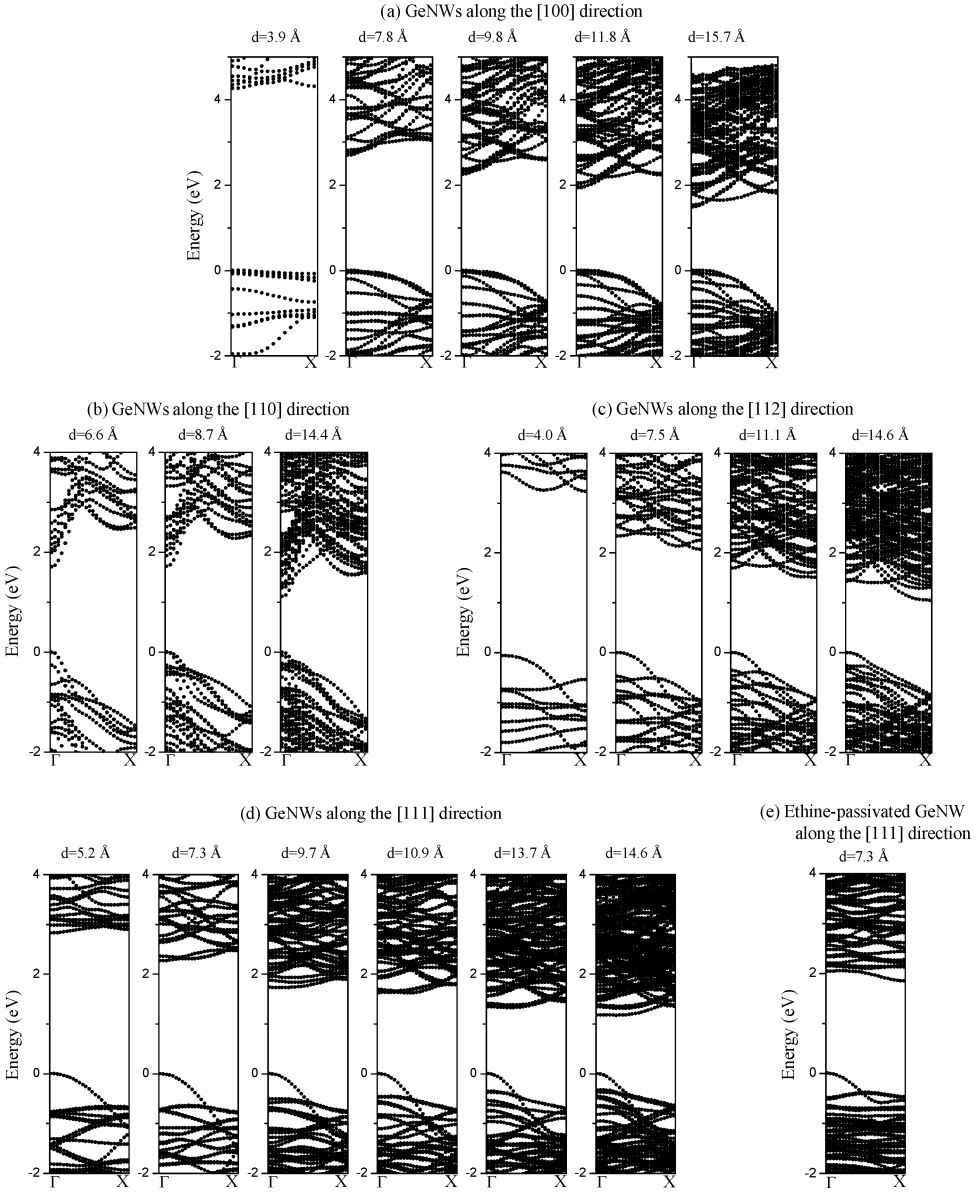

Figure 2. Electronic structures of the fully relaxed H-passivated GeNWs along the (a) [100], (b) [110], (c) [112], and (d) [111] directions. The electronic structure of the fully relaxed ethine-passivated [111]-oriented GeNW with $d = 7.3$ Å is shown in panel (e). The valence band top is set to zero.

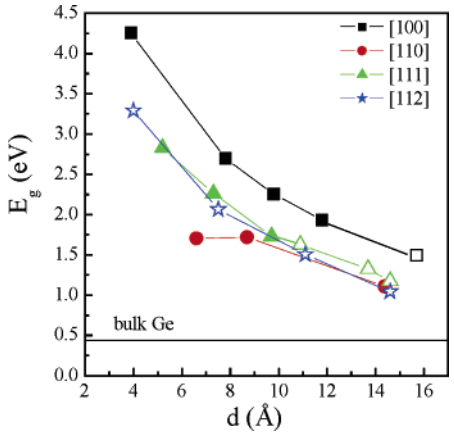

Figure 3. (Color online) Energy gap E_g of the H-passivated GeNWs along the four directions as a function of the wire size d. The solid and empty symbols represent the direct and indirect band gaps, respectively.

GeNWs have direct band gaps, whereas the [100]- and [111]-oriented GeNWs are characterized by an indirect band gap. The energy difference between the direct and indirect gaps is small for the [100]- and [111]-oriented GeNWs. Unfortunately, the H-passivated GeNWs suffer from an extreme instability in the presence of oxygen.[28,29] On the other hand, functionalization by alkanethiols, alkyl, alkene, and alkyne can significantly improve the stability of GeNWs in the air. But the effects of different chemical passivation patterns on the electronic structures of GeNWs remain open. Besides, the higher-index [112]-orientated GeNWs have been synthesized,[16] but no corresponding theoretical work is reported for them.

In this article, we have investigated the orientation and passivation dependence of quantum confinement effects of the fully relaxed H-passivated [100]-, [110]-, [111]-, and [112]-orientated GeNWs in a larger wire width range of 4−16 Å by using DFT within the generalized gradient approximation (GGA).[30] The band gaps of GeNWs along the [112] direction turn out to be indirect. The band gap enhancement of GeNWs owing to quantum confinement effects is generally larger than that of similar-sized SiNWs, confirming the larger quantum confinement effects in Ge than in Si when they are confined in

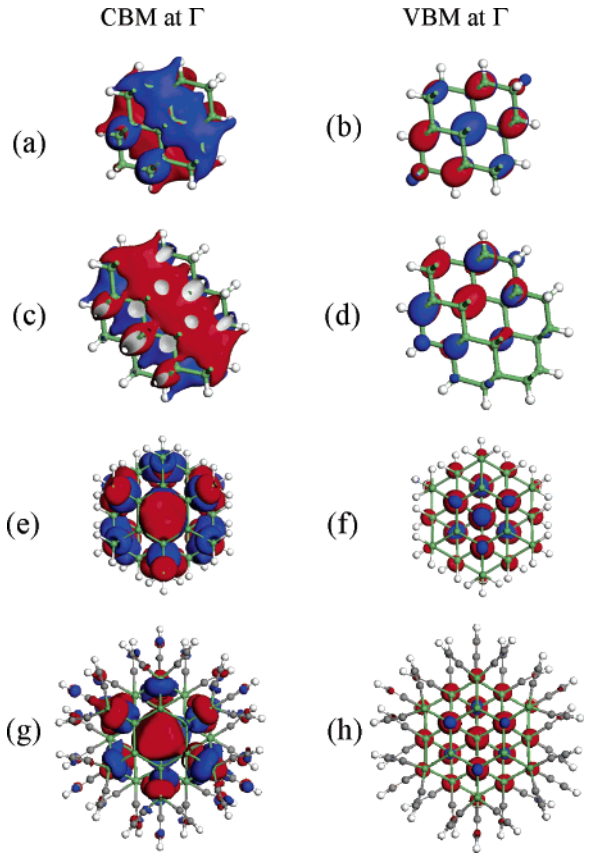

Figure 4. (Color online) Wave functions of the CBM (left) and VBM (right) at the Γ point of the H-passivated [110]-oriented GeNWs with $d = 6.6$ (a,b) and 8.7 Å (c,d) and the H-passivated (e,f) and C_2H-passivated (g,h) [111]-oriented GeNWs with $d = 7.3$ Å. Red and blue represent positive and negative regions, respectively. The isovalue is 0.014 and 0.025 au for the CBM and VBM, respectively.

two dimensions. Investigation of one ethine-passivated GeNW along the [111] direction shows that the stable chemical passivation leads to a weakening of quantum confinement effects compared with the hydrogen passivation.

Model and Method

The models of the GeNWs with a Ge crystalline core along the [100], [110], [111], and [112] directions are shown in Figure 1. The original wires are generated from bulk Ge by cutting the outside part of a circle with a selected radius. The GeNWs along the [100] direction have quadrate cross sections; they are labeled as $N \times N$, where N is the Ge atom number on each side. For the [111]-oriented wires, the shape of the cross section alternates between stars and hexagons as the size decreases continually. Limited by the computational cost, for chemical stable passivation, we consider only one ethine-terminated [111]-oriented GeNW with $d = 7.3$ Å, which is shown in Figure 1e.

Periodic boundary conditions are employed in the $x-y$ plane, forming a hexagonal cell. A 6-Å separation between the two closest H atoms on neighboring wires is sufficient to make interaction negligible. Full geometry optimization is performed for the atomic positions and the wire axis (z-direction) by using the ultrasoft pseudopotentials[31] plane-wave program, CASTEP,[32] with a cutoff energy of 180 eV. The x- and y-directions of the supercell are fixed during optimization. The convergence criteria of energy and force are 10^{-5} eV/atom and 10^{-2} eV/Å, respectively. The $1 \times 1 \times 4$, $1 \times 1 \times 5$, $1 \times 1 \times 2$, and $1 \times 1 \times 3$ Monkhorst−Pack k-point meshes[33] are used for the Brillouin zone sampling of the GeNWs along the [100], [110], [111], and [112] directions, respectively. As for the ethine-passivated GeNW, a $1 \times 1 \times 2$ k-point mesh is used for the Brillouin zone sampling. The electronic band structures of the GeNWs are calculated with all electron double numerical plus d-functions (DND) atomic orbital basis set implemented in DMOL package.[34] This numerical atomic orbital basis set method can generate a band structure quite similar to that generated by the ultrasoft plane-wave basis set method but with much less computation cost.

Results and Discussion

A. Hydrogen-Passivated GeNWs. The calculated periodicity of bulk Ge by using a $11 \times 11 \times 11$ Monkhorst−Pack k-point mesh and 180-eV plane-wave cutoff energy is 5.55 Å, which is 0.1 Å smaller than the experimental value. The calculated periodicity of bulk Ge along the [100], [110], [111], and [112] directions is 5.55, 3.92, 9.61, and 6.80 Å, respectively. The variation of these periodicities is dependent on the direction, the size, and the passivation pattern of GeNWs. Generally speaking, the smaller-sized wires undergo a larger variation. The average changes in periodicity of the examined H-terminated GeNWs along the [100], [110], [111], and [112] directions are −0.2, 1.0, −0.6, and −0.5%, respectively, compared with optimized bulk Ge.

The electronic band structures of the H-passivated GeNWs along the four directions are shown in Figure 2, and the size dependence of the fundamental band gap is shown in Figure 3. The fundamental band gap basically increases with decreasing size along each direction except that the band gap (1.70 eV) of the [110]-oriented wire at $d = 6.6$ Å is 0.02 eV smaller than that at $d = 8.7$ Å. Orbital analysis shows that the surface hydrogen atoms contribute only slightly to the conduction band minimum (CBM) (Figure 4c) of the [110]-oriented GeNW with $d = 8.7$ Å, while keeping its valence band maximum (VBM) intact (Figure 4d). However, the surface hydrogen atoms not only slightly contribute to the VBM (Figure 4b) but also moderately contribute to the CBM (Figure 4a) of the [110]-oriented GeNW with $d = 6.6$ Å. Therefore, the weakened quantum confinement effects in the [110]-oriented GeNW with $d = 6.6$ Å compared with that with $d = 8.7$ Å is attributed to the enhanced surface effect due to its extremely small size.

All the examined [110]-oriented wires have a direct band gap at the Γ point, a result consistent with previous works.[26,27] The [112]-oriented wires have an indirect band gap even as the size decreases to 3.9 Å. In contrast to previous works,[26,27] we find that the energy gaps of both the [100]- and [111]-oriented GeNWs are direct at sizes of less than 12 Å and 10 Å, respectively. Beyond these sizes, the VBM of the [100]-oriented GeNWs and the CBM of the [111]-oriented GeNWs are shifted away from the Γ point, which results in an indirect fundamental band gap. However, the energy difference between the direct and indirect band gaps is smaller than 0.02 eV for these investigated larger-sized [100]- and [111]-oriented GeNWs. It is worth noting that the energy gaps of the [100]- and [111]-oriented SiNWs are also calculated to be direct at small sizes.[6−10]

We have investigated in detail the dependence of the lattice constant and energy gap of the 3×3 [100]-oriented GeNW with $d = 3.9$ Å on the exchange-correlation functional, the number of k-point, the pseudopotential, and the cutoff energy used in the optimization. The results are provided in Figure 5 and Table 1. When the lattice constant is relaxed ($c = 5.44-5.55$ Å, compared with an unrelaxed value of 5.65 Å), we always obtain a direct band gap. The difference between the direct and indirect band gap is even greater in LDA calculations than in

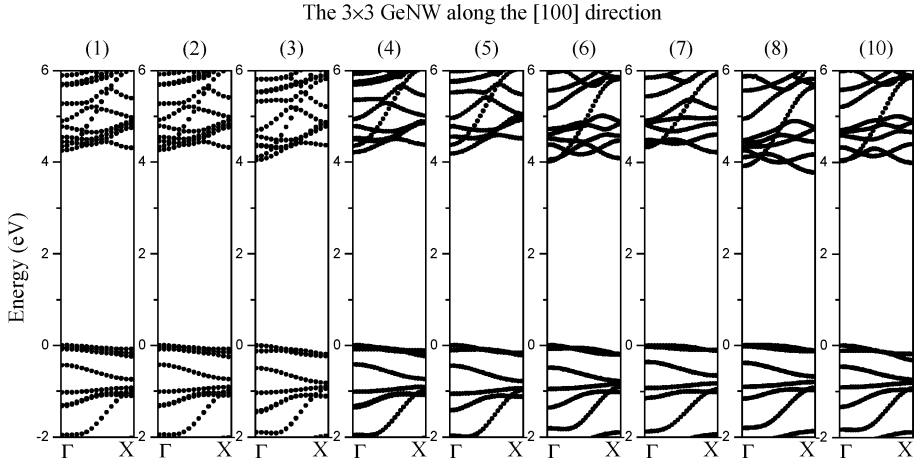

Figure 5. Electronic structures of the 3 × 3 [100]-oriented GeNW with $d = 3.9$ Å obtained in different schemes. The parameter sets of these schemes are referred to Table 1. The valence band top is set to zero.

TABLE 1: Dependence of the Lattice Constant (Å) and Energy Gap (eV) of the 3 × 3 [100]-oriented GeNW with $d = 3.9$ Å on the Parameter Sets[a]

scheme	functional	program	*k*-point setting[b]	cutoff energy (eV)	pseudopotential	lattice constant	band gap	gap feature	δ^d (eV)
1	GGA	CASTEP	4	180[b]	ultrasoft	5.54	4.25	direct	−0.05
2	GGA	CASTEP	9	180[b]	ultrasoft	5.55	4.26	direct	−0.06
3	LDA	CASTEP	9	180[b]	ultrasoft	5.48	4.04	direct	−0.33
4	LDA	CASTEP	9	260[b]	ultrasoft	5.53	4.21	direct	−0.17
5	LDA	CASTEP	9	500[b]	normconserving	5.44	4.19	direct	−0.33
6	LDA	ABINIT	8	400[b]	normconserving	5.52	4.01	direct	−0.07
7	GGA	DMOL			all electron	5.65	4.20	indirect	0.19
8	LDA	ABINIT		400[c]	normconserving	5.65	3.78	indirect	0.14
9[e]	LDA	WIEN97			all electron LAPW	5.65	4.10	indirect	0.20
10	LDA	ABINIT	8	400[b,c]	normconserving	5.65	3.98	indirect	0.04
11[f]	LDA	ABINIT	8	400[b,c]	normconserving	5.65	3.90	indirect	

[a] The band structures in schemes 1−6 are generated by using the DND basis set; in schemes 7−9, the geometry comes directly from a cutting of bulk Ge; in schemes 10 and 11, only the atomic positions are relaxed. [b] Optimization parameter. [c] Band structure calculation parameter. [d] The difference between the indirect and direct band gaps; the direct band gap is defined as from the VBM at Γ to the CBM at Γ. [e] Ref 26. [f] Ref 27.

GGA ones. On the other hand, the previously reported[26,27] indirect band gap is well reproduced when the lattice constant is not relaxed. Therefore, the discrepancy between the previous[26,27] and the present calculations is attributed to whether the lattice constants of the [100]- and [111]-oriented GeNWs are relaxed. In view of the lattice-constant error between DFT (5.55 Å) and experimental value (5.65 Å) for bulk Ge, the electronic structure from the fully relaxed GeNW is not necessarily more reliable than that without relaxing the lattice constant. Now that the electronic structures of the [100]- and [111]-oriented GeNWs are sensitive to their lattice constant, it is possible to control the electronic properties and thus optical properties of the two types of GeNWs by stretching or compressing their wire axis.

It was shown in the previous works[26,27] that the magnitude of the band gaps of the GeNWs along the different orientations for a given size follows the order of $E_g[100] > E_g[111] > E_g[110]$. In our calculations, the magnitude of the band gaps along the different wire orientations for a given size approximately follows the order of $E_g[100] > E_g[111] > E_g[112] > E_g[110]$.

B. Comparison of the Electronic Structure Between Hydrogen-Passivated GeNWs and SiNWs. The measured (0.74 eV) and calculated (0.43 eV) band gaps of bulk Ge are 0.43 and 0.21 eV smaller than those of bulk Si, respectively. The band gaps of the SiNWs along the [100], [110], [111], and [112] directions are calculated at the same level and are compared with the GeNWs in Figure 6. The band gap feature (direct or indirect) and magnitude of the two types of nanowires are fairly similar. Both of them have a direct band gap along the [100] and [110] directions at $d < 15$ Å. Along the [112] direction, the band gaps of the two wires are always indirect. Along the [111] direction, the two wires have direct gaps at $d < 8$ Å and indirect gaps at $d > 10$ Å.

The average band gap difference between the examined similar-sized GeNWs and SiNWs, E_g(GeNW) − E_g(SiNW), along the [100], [110], [111], and [112] direction is −0.04, −0.16, −0.14, and −0.13 eV, respectively. The average band gap difference over all the examined similar-sized GeNWs and SiNWs is −0.12 eV, smaller than a difference of −0.21 eV between bulk Ge and Si. It implies that the average energy gap enhancement ΔE_g due to the quantum confinement effects relative to bulk material in the GeNWs is larger than in the SiNWs. Figure 7 displays the energy gap enhancement ΔE_g of the GeNWs (blue squares) and SiNWs (red circles) relative to their respective bulk materials as a function of the wire size *d*. The values of ΔE_g of the GeNWs are indeed generally larger than those of the similar-sized SiNWs. Taking the [100] direction as an example, the values of ΔE_g of the GeNWs are 0.21, 0.21, 0.22, and 0.08 eV larger than those of the similar-sized SiNWs at $d \approx 7.7$, 9.7, 11.6, and 15.5 Å, respectively. The quantum confinement effects are therefore stronger in GeNWs than in SiNWs.

C. Ethine-Passivated GeNW. After geometry optimization, the periodicity along the wire axis of the C_2H-passivated [111]-oriented GeNW with $d = 7.3$ Å changes into 9.71 Å, 1.0% larger than that in the optimized bulk Ge along the [111]

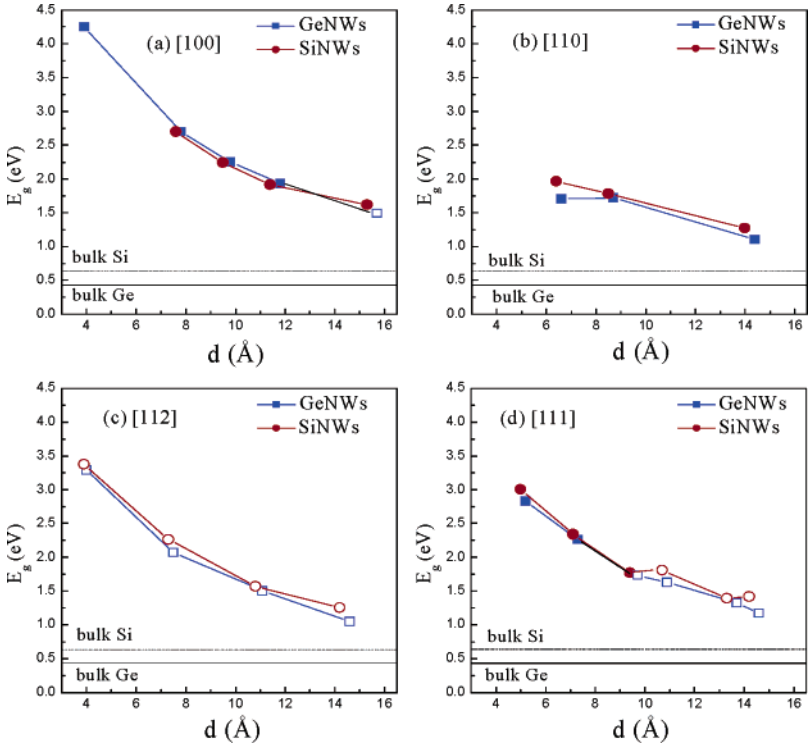

Figure 6. (Color online) Comparison of the energy gaps calculated with the same level for GeNWs (blue squares) and SiNWs (red circles). The calculated energy gaps of bulk Ge (solid line) and Si (dash−dot line) are shown in the bottom. The solid and empty symbols represent the direct and indirect band gaps, respectively.

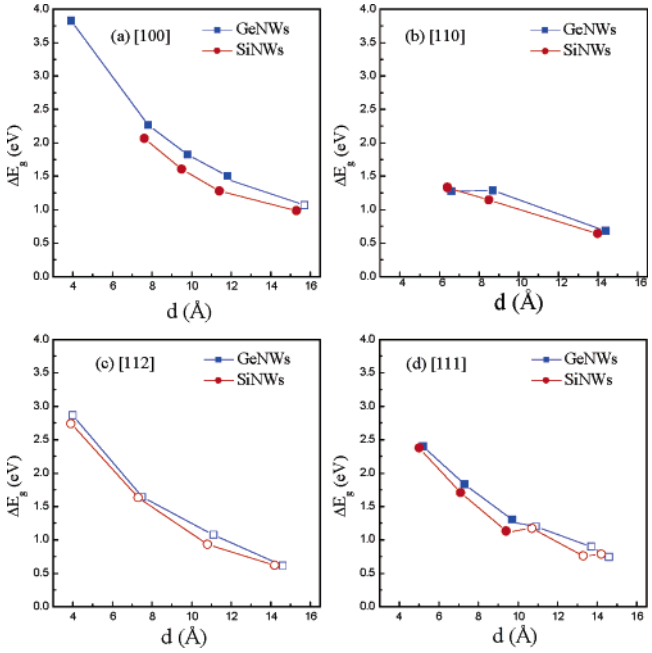

Figure 7. (Color online) Energy gap enhancement ΔE_g of the GeNWs (blue squares) and SiNWs (red circles) relative to their respective bulk materials as a function of the wire size d. The solid and empty symbols represent the direct and indirect band gaps, respectively.

direction and 1.8% larger than that of the H-passivated counterpart. The calculated binding energy of C_2H and H to the GeNW is −5.64 and −4.58 eV, respectively, a result consistent with the reported higher stability of C_2H-passivated GeNWs versus H-passivated ones.[28,29]

The electronic structure of the ethine-terminated GeNW is shown in Figure 2e. The VBM is still located at the Γ point, but the CBM is shifted from the Γ to the X point and gives rise to an indirect fundamental band gap, whose magnitude (1.82 eV) is 18.2% smaller than that of the corresponding H-passivated GeNW. Therefore, the quantum confinement effects are weakened in the ethine-terminated GeNW relative to the H-terminated counterpart. Figure 4e−h provides a comparison of the wave functions of the CBM and VBM at the Γ point of the H- and C_2H-passivated [111]-oriented GeNWs with $d = 7.3$ Å. The hydrogen atoms contribute to neither the CBM nor the VBM of the GeNW. However, the C_2H groups not only moderately contribute to the CBM (Figure 4g) but also slightly contribute to the VBM of the GeNW (Figure 4h). The weakening of the quantum confinement effects in the C_2H-passivated GeNW is thus ascribed to the nontrivial contribution of the C_2H groups to the conduction and valence bands of the GeNW.

Conclusions

In summary, the structures and electronic energy bands of the H-passivated GeNWs along the [100], [110], [111], and [112] directions are investigated by means of the density functional theory within the generalized gradient approximation. The magnitude of the band gaps of the GeNWs for a given size approximately follows the order of $E_g[100] > E_g[111] > E_g[112] > E_g[110]$. Similar to the SiNWs, the band gaps of the GeNWs along the [100], [110], and [111] directions are all direct at the smaller sizes while those of the wires along the [112] direction remain indirect. Remarkably, GeNWs exhibit stronger quantum confinement effects than SiNWs. The surface effects are found to weaken the quantum confinement effects in the very thin H-passivated [110]-oriented GeNW and the C_2H-passivated [111]-oriented GeNW.

Acknowledgment. This work was supported by the NSFC (Grant Nos. 10474123, 10434010, and 20131040), national 973 projects (No. 2002CB613505, MOST of China), 985 Project and Creative Team Project of MOE of China and Nebraska

Research Initiative (No. 4132050400) of USA. Our calculations were partially carried out in the HP Cluster of the Calculation Center of Science and Engineering of Peking University.

References and Notes

(1) Alivisatos, A. P. *Science* **1996**, *271*, 933.
(2) Gulseren, O.; Ercolessi, F.; Tosatti, E. *Phys. Rev. Lett.* **1998**, *80*, 3775.
(3) Morales, A. M.; Lieber, C. M. *Science* **1998**, *279*, 208.
(4) Holmes, J. D.; Johnston, K. P.; Doty, R. C.; Korgel, B. A. *Science* **2000**, *287*, 1471.
(5) Ma, D. D. D.; Lee, C. S.; Au, F. C. K.; Tong, S. Y.; Lee, S. T. *Science* **2003**, *299*, 1874.
(6) Read, A. J.; Needs, R. J.; Nash, K. J.; Canham, L. T.; Calcott, P. D. J.; Qteish, A. *Phys. Rev. Lett.* **1992**, *69*, 1232.
(7) Ohno, T.; Shiraishi, K.; Ogawa, T. *Phys. Rev. Lett.* **1992**, *69*, 2400.
(8) Hybertsen, M. S.; Needels, M. *Phys. Rev. B* **1993**, *48*, 4608.
(9) Needs, R. J.; Bhattacharjee, S.; Nash, K. J.; Qteish, A.; Read, A. J.; Canham, L. T. *Phys. Rev. B* **1994**, *50*, 14223.
(10) Zhao, X. Y.; Wei, C. M.; Yang, L.; Chou, M. Y. *Phys. Rev. Lett.* **2004**, *92*, 236805.
(11) Bhattacharya, S.; Banerjee, D.; Adu, K. W.; Samui, S.; Bhattacharyya, S. *Appl. Phys. Lett.* **2004**, *85*, 2008.
(12) Maeda, Y.; Tsukamoto, N.; Yazawa, Y.; Kanemitsu, Y.; Masumoto, Y. *Appl. Phys. Lett.* **1991**, *59*, 3168.
(13) Cullis, A. G.; Canham, L. T.; Calcott, P. D. J. *J. Appl. Phys.* **1997**, *82*, 909.
(14) Bostedt, C.; Buuren, T.; Willey, T. M.; Franco, N.; Terminello, L. J.; Heske, C.; Moller, T. *Appl. Phys. Lett.* **2004**, *84*, 4056.
(15) Omi, H.; Ogino, T. *Appl. Phys. Lett.* **1997**, *71*, 2163.
(16) Zhang, Y. F.; Tang, Y. H.; Wang, N.; Lee, C. S.; Bello, I.; Lee, S. T. *Phys. Rev. B* **2000**, *61*, 4518.
(17) Halsall, M. P.; Omi, H.; Ogino, T. *Appl. Phys. Lett.* **2002**, *81*, 2448.
(18) Palummo, M.; Onida, G.; Del Sole, R.; Stella, A.; Tognini, P.; Cheyssac, P.; Kofman, R. *Phys. Status Solidi B* **2001**, *224*, 247.
(19) Hill, N. A.; Pokrant, S.; Hill, A. J. *J. Phys. Chem. B* **1999**, *103*, 3156.
(20) Palummo, M.; Onida, G.; Del Sole, R. *Phys. Status Solidi A* **1999**, *175*, 23.
(21) Reboredo, F. A.; Zunger, A. *Phys. Rev. B* **2000**, *62*, R2275.
(22) Melnikov, D. V.; Chelikowsky, J. R. *Phys. Rev. B* **2004**, *69*, 113305.
(23) Kholod, A. N.; Saul, A.; Fuhr, J. D.; Borisenko, V. E.; d'Avitaya, F. A. *Phys. Rev. B* **2000**, *62*, 12949.
(24) Kholod, A. N.; Ossicini, S.; Borisenko, V. E.; d'Avitaya, F. A. *Phys. Rev. B* **2002**, *65*, 115315.
(25) Kholod, A. N.; Ossicini, S.; Borisenko, V. E.; d'Avitaya, F. A. *Surf. Sci.* **2003**, *527*, 30.
(26) Kholod, A. N.; Shaposhnikov, V. L.; Sobolev, N.; Borisenko, V. E.; D'Avitaya, F. A.; Ossicini, S. *Phys. Rev. B* **2004**, *70*, 035317.
(27) Bruno, M.; Palummo, M.; Marini, A.; Del Sole, R.; Olevano, V.; Kholod, A. N.; Ossicini, S. *Phys. Rev. B* **2005**, *72*, 153310.
(28) Hanrath, T.; Korgel, B. A. *J. Am. Chem. Soc.* **2004**, *126*, 15466.
(29) Wang, D. W.; Chang, Y. L.; Wang, Q.; Cao, J.; Farmer, D. B.; Gordon, R. G.; Dai, H. J. *J. Am. Chem. Soc.* **2004**, *126*, 11602.
(30) Perdew, J. P.; Chevary, J. A.; Vosko, S. H.; Jackson, K. A.; Pederson, M. R.; Singh, D. J.; Fiolhais, C. *Phys. Rev. B* **1992**, *46*, 6671.
(31) Vanderbilt, D. *Phys. Rev. B* **1990**, *41*, 7892.
(32) Milman, V.; Winkler, B.; White, J. A.; Pickard, C. J.; Payne, M. C.; Akhmatskaya, E. V.; Nobes, R. H. *Int. J. Quantum Chem.* **2000**, *77*, 895.
(33) Monkhorst, H. J.; Pack, J. D. *Phys. Rev. B* **1976**, *13*, 5188.
(34) Delley, B. *J. Chem. Phys.* **2000**, *113*, 7756.